European Journal of Medical Genetics 66 (2023) 104693

Contents lists available at ScienceDirect

European Journal of Medical Genetics

journal homepage: www.elsevier.com/locate/ejmg

UNC45A-related osteo-oto-hepato-enteric syndrome in a Chinese neonate

Ying Kong [a,1], Chaoqun Ye [a,1], Leyang Shi [a], Qingmei Dai [a], Ying Wang [a], Jun Hu [b], Xueyan Wu [c], Meiyu Shi [d], Xiaofeng Hu [e,**], Huizhi Huang [a,*]

[a] Department of Neonatology, Anhui Provincial Children's Hospital/Children's Hospital Affiliated to Anhui Medical University, Hefei, China
[b] Department of Radiology, Anhui Provincial Children's Hospital, Hefei, China
[c] School of Basic Medical Sciences, Anhui Medical University, Hefei, China
[d] School of Life Sciences, University of Science and Technology of China, Hefei, China
[e] Department of Radiology, The First Affiliated Hospital of USTC, Division of Life Sciences and Medicine, University of Science and Technology of China, Hefei, China

ARTICLE INFO

Handling Editor: A. Verloes

Keywords:
Osteo-oto-hepato-enteric syndrome
OOHE
UNC45A
MYO5B
Gene testing

ABSTRACT

Unexplained diarrhea and cholestasis are common clinical phenotypes in newborns, indicating there is only a little common genetic basis for these conditions. However, it has been reported that defects in the *UNC45A* gene can lead to osteo-oto-hepato-enteric syndrome. However, to date, only 10 patients with this syndrome have been reported in 2 studies; therefore, there is still a lack of analysis regarding the correlation between disease phenotype and genotype. Trio-whole exome sequencing was conducted using DNA samples from a newborn with congenital diarrhea and cholestasis from a Chinese Han family. The *UNC45A* variants were verified using Sanger sequencing. In addition, we applied a crystal structure model to analyze the potential hazards associated with the variants. The plasmids were constructed *in vitro* and transfected into human 293T cells for Western blot (WB) analysis. After the mutant protein was fused with the Green Fluorescent Protein label, intracellular localization was observed using laser confocal microscopy. The gene detection results showed that the *UNC45A* gene of the newborn examined in the present study harbored the compound heterozygous variants p.Arg819Ter, and p.Leu237Pro; this was confirmed via Sanger sequencing. Analysis of the Leu237Pro crystal structure model suggested that this variant may decrease local structural stability and affect protein function. The Western blot and laser confocal microscopy observation results suggested that the Leu237Pro mutation leads to reduced protein expression, while the Arg819Ter mutation completely inhibits the expression of the protein. The compound heterozygous variants of *UNC45A* (p.Arg819Ter and p.Leu237Pro) may be pathogenic factors of congenital diarrhea and cholestasis in this neonatal patient. Therefore, *UNC45A* deficiency should be considered when intractable diarrhea and cholestasis occur in newborns.

1. Introduction

Congenital diarrhea and cholestasis are common digestive system or hepatobiliary diseases in newborns and infants. However, the etiology of these symptoms is complex, and it is necessary to distinguish between diarrhea and various other diseases with similar or overlapping phenotypes, such as microvillus inclusion disease (MVID), and consequently, accurate diagnose such diseases. Therefore, diagnosis based on clinical features, biochemical indicators, radiological features, and histopathology has become challenging (Balistreri et al., 2005; Fawaz et al., 2017). Congenital diarrhea (CDDs) can cause life-threatening symptoms, mainly in the neonatal stage. However, the causes of diarrhea are complex and may be related to digestive disorders, intestinal immunity, and other factors (Esposito., 2021). In contrast, biliary atresia is the most common cause of cholestasis. Approximately 25–50% of cases can be explained by single gene defects, and the functions of these genes are mainly related to direct or indirect factors of physiological processes, such as bile production, transportation, and excretion

* Corresponding author. Department of Neonatology, Anhui Provincial Children's Hospital/Children's Hospital affiliated to Anhui Medical University, Hefei, 230022, China.
** Corresponding author. Department of Radiology, The First Affiliated Hospital of USTC, Division of Life Sciences and Medicine, University of Science and Technology of China, Hefei, 30002, China.
E-mail addresses: hxf0296@126.com (X. Hu), ach_huanghuizhi@163.com (H. Huang).
[1] These authors have contributed equally to this work and share first authorship.

https://doi.org/10.1016/j.ejmg.2022.104693
Received 4 July 2022; Received in revised form 23 November 2022; Accepted 29 December 2022
Available online 30 December 2022

(Goldberg and Mack, 2020; Feldman and Sokol, 2013).

However, there are only a few studies regarding the common genetic basis of CDDs and cholestasis in newborns and infants. Esteve et al. found a biallelic *UNC-45A* variant in four patients with congenital cholestasis, diarrhea, repeated fractures, and deafness in three families in 2018 and called this disease the osteo-oto-hepato-enteric syndrome (OOHE, OMIM#619377) (Esteve et al., 2018). *UNC-45A* encodes an uncoordinated-45a myosin chaperone protein. Its participation in the biological functions of the human hepatobiliary and gastrointestinal systems remains largely unknown (Barral et al., 2002). To date, only ten OOHE patients have been reported worldwide, and 13 *UNC-45A* variants related to the disease have been reported. Therefore, there is a lack of research regarding this rare disease, especially, clinical reports of neonatal patients with this condition (Esteve et al., 2018; Duclaux-Loras et al., 2022).

In the present study, we report a newborn with OOHE and analyze the biological hazards of two *UNC-45A* variants. To the best of our knowledge, this is the first patient with OOHE in China. This study focused on the disease characteristics of newborns with OOHE and further expanded the *UNC-45A* variation spectrum.

2. Materials and methods

2.1. Subjects

The patient who participated in this study came from a non-consanguineous family and was admitted to the Anhui Children's Hospital Department of Neonatology. All studies were approved by the Medical Ethics Committee of the Anhui Children's Hospital.

2.2. Gene analysis

After the patient's parents signed the informed consent form, the patient and her parents were tested using trio-whole exome sequencing (trio-WES). After collecting 3 mL of peripheral blood from family members (EDTA tube anticoagulation treatment), leukocyte DNA was extracted according to the instructions of the genome extraction kit (CwBio, Beijing, China). After the library was constructed, the designed sequence was captured by the Illumina NoveSeq 6000 high-throughput sequencer (Illumina, San Diego, CA, USA). For the screened variants, the distribution databases of the normal population, including dbSNP (www.ncbi.nlm.nih.gov/snp), ExAC (www.exac.broadinstitute.org/), and 1000 Genome (www.1000genomes.org) databases, and GATK software were used to analyze the single nucleotide variant, insertion-deletion, and other variants. After filtering out the invalid variants, the hazard associated with a reliable variation spectrum was predicted and analyzed (SIFT [www.sift.bii.a-star.edu.sg], Polyphen2 [www.genetics.bwh.harvard.edu/pph2], and MutationTaster [www.mutationtaster.org] online software). For suspected variants, primers were designed according to the Ensemble database (http://ensemblgenomes.org/), and Sanger verification was performed with an ABI 3500XL analyzer. Finally, the American College of Medical Genetics (ACMG) guidelines were used to rate the pathogenicity of the variants (Richards et al., 2015).

2.3. Prediction and analysis of crystal structure

The human UNC-45A amino acid sequence file (UniProtKB - Q9H3U1) was retrieved from the UniProt database (https://www.uniprot.org/), and the sequences of several species were compared for conservative analysis. The Robetta online protein structure prediction server was used to predict the three-dimensional structure of wild-type and variant proteins (https://robetta.bakerlab.org/) (Baek et al., 2021). A three-level structure with a complete structure was constructed by comparing the modeling templates and restricting the modeling conditions. The variant structure was constructed on the wild-type model, analyzed, and displayed using PyMOL version 2.3.

2.4. Cell culture and plasmid construction

Human 293T cells (Shanghai Cell Bank) were cultured in high-glucose Dulbecco's modified Eagle's medium (DMEM; GIBCO, USA) containing 10% fetal serum. The cells were cultured at 37°C under 5% CO_2 conditions; the plasmid was transfected with Lip2000 (Thermo Scientific, Waltham, MA, USA) when the cell density reached 60% in a 6-well plate. The pECMV-3 × FLAG-N and pCDNA3.1-gfp-1 vectors were used to construct UNC45A-WT with the wild-type plasmid according to the instructions of Phanta® Max Super-Fidelity DNA Polymerase (Vazyme #P505). The mutant plasmid was constructed according to the instructions of the Mut Express MultiS Fast Mutagenesis Kit V2 (Vazyme #C215) to generate UNC45A-MUT. The primer sequences used for amplification are listed in Table 1. After verification by Sanger sequencing, plasmids were amplified and extracted.

2.5. Western blotting (WB)

The total protein of human 293T cells was extracted with radioimmunoprecipitation assay (RIPA) buffer (Beyotime, China) 48 h after transfection, and the protein concentration was measured with the Multiskan MK3 (Thermo Scientific, Waltham, MA, USA). After high-temperature denaturation, the protein was separated using 10% sodium dodecyl sulfate-polyacrylamide gel electrophoresis. After transfer, the polyvinylidene fluoride membrane (Bio-Rad, USA) was incubated with the primary antibody (mouse anti-human flag, CST cat#8146, 1:1000; mouse anti-human β- Actin, CST, cat#3700, 1:1000) at 25°C for 2 h, and then with the secondary antibody (anti-mouse IgG, HRP-linked antibody, CST, cat#7076, 1:5000) for 1 h. Then the chemiluminescence system (Tianneng, Shanghai) was used for detection. ImageJ software was used to analyze the average fluorescence intensity of the proteins in the cells.

2.6. Observation of protein localization by laser confocal microscopy

After fusing the C terminal of the UNC45A protein with the green fluorescent protein (GFP) tag, the protein localization can be observed using laser confocal microscopy, and the protein expression can be indirectly reflected. 293T cells that grew well after transfection in confocal Petri dishes (Biosharp, #BS-20-GJM, Hefei, China) were fixed with 4% paraformaldehyde tissue fixative (Biosharp, #BL539A, Hefei, China) for 20 min, washed with PBS, and stained with an appropriate amount of DAPI staining solution (Beyotime, #C1005, Shanghai, China); the stained samples were visualized using a confocal microscope (1000 × magnification).

Table 1
Primer sequence information involved in plasmid construction.

Construction of UNC45A-WT amplification primer sequence with wild-type plasmid
F1: 5′- ctcaccatggtggcgaccggtAGCTTGGTACCGAGCTCGG -3′
R1: 5′- tcacagtcatGGACCCACCACCGCCCTT -3′
F2: 5′- tggtgggtccATGACTGTGAGTGGTCCAGGGA -3′
R2: 5′- ctagcgtttaaacttaagcttCTCTCCATCTTGGTTGGGTTGG -3′
UNC45A-MUT amplification primer sequence with variant plasmid (Leu237Pro)
F:5′- TGAGCATACcGGGAACTCGGCGAGTAGTCTCC -3′
R: 5′- AGTTCCCgGTATGCTCAGGGTTGCCACTGTCC -3′
UNC45A-MUT amplification primer sequence with variant plasmid (Arg819Ter)
F: 5′- GCAATGACtGACTGAAGCTGCTGGTGCTGTAC -3′
R: 5′- CTTCAGTCaGTCATTGCCCTGGGCTTCGAAGA -3′

F: Forward sequence; R: Reverse sequence.

3. Results

3.1. Case presentation

This patient was a female infant less than 1 day old. She was her mother's first child and was delivered vaginally at 35 + 1 weeks of pregnancy because of a fetal membrane rupture. Her birth weight was 2050 g (z-score: 2.88). The Apgar scores at 1 and 5 min were 7 and 8, respectively. Her amniotic fluid volume was normal, and she had grade II pollution. She was admitted to another hospital because of a poor reaction and weak crying after premature birth. Later, the baby was transferred to the neonatal department of the Anhui Children's Hospital because of severe diarrhea (10 days after birth, height 48 cm [z-score: 0.61], weight 3380 g [z-score: 3.78], head circumference 36 cm [z-score: 1.75]) (Van den Broeck., 2009). During the course of the disease, the stool was green-white or white loose, and there was no abnormal urination. Physical examination on admission showed weak crying, clear consciousness, general skin elasticity, floral changes, mild yellow staining, and no other evident abnormalities.

Routine blood examination showed that the number of leukocytes and neutrophils had increased, and the hemolytic screening test of newborns showed ABO hemolysis. Analyses of biochemical indicators showed that the levels of total bile acid, total bilirubin, direct bilirubin, and indirect bilirubin were considerable increased and those of aspartate aminotransferase were slightly increased; these results and the results of other auxiliary examinations are shown in Table 2. The chest and abdominal X-ray examination showed that the abdominal bowel was insufficiently inflated, and a part of the bowel was slightly inflated and expanded. Color Doppler ultrasonography of the liver, gallbladder, pancreas, spleen, and urinary system showed separation of the left kidney and renal pelvis, without biliary atresia. Color Doppler echocardiography showed an atrial/ventricular septal defect and pulmonary hypertension. Color Doppler ultrasound examination showed that the brain was immature with bilateral intraventricular hemorrhage and bilateral ventricular widening. Magnetic resonance cholangiopancreatography (MRCP) showed that the gallbladder volume increased (Fig. 1a).

Table 2
Laboratory data of the patient in this study.

Test items	Patient data	Reference range
Routine blood test		
white blood cell (× 10^9/L)	21.58	5.60–14.50
neutrophils (× 10^9/L)	9.88	7.00–51。00
lymphocyte (× 10^9/L)	7.76	34.00–81.00
red blood cell (× 10^12/L)	5.03	3.50–5.60
hematocrit (%)	55.4	29.0–57.0
hemoglobin (g/L)	180	99–196
platelet (× 10^9/L)	443	203–653
C-reactive protein (mg/L)	1.49	0–2.00
Biochemical detection		
total bilirubin (μmol/L)	150.7	2.0–21.0
direct bilirubin (μmol/L)	65.3	0–8.0
indirect bilirubin (μmol/L)	85.4	2.0–18.0
glutamyl transpeptidase (IU/L)	0	9–150
total bile acid (μmol/L)	166	0–20
total protein (g/L)	78.4	49.0–71.0
albumin (g/L)	47.4	35.0–50.0
globulin (g/L)	31.0	9.0–27.0
ALT (U/L)	17.0	7.0–71.0
AST (U/L)	168.0	21.0–80.0
AST/ALT	9.88	1.90–2.20
Blood electrolyte detection		
potassium ion (mmol/L)	8.20	4.10–5.60
sodium ion (mmol/L)	123.00	135.00–145.00
iron ion (mmol/L)	8.70	7.34–28.60

ALT: alanine aminotransferase; AST: aspartate aminotransferase.

3.2. Gene detection results showed a biallelic UNC-45A variant

The results of trio-WES showed that, in this patient, the *UNC-45A gene* had compound heterozygous variants NM_018671: c.2455C>T(p.Arg819Ter) and c.710T>C(p.Leu237Pro), in which p.Arg819Ter was inherited from the father and p.Leu237Pro was inherited from the mother. No other genetic bilirubinemia or cholestasis gene variants were found. Searching the dbSNP, ExAC, and 1000 Genome databases suggested that p.Arg819Ter and p.Leu237Pro were not included. SIFT, Polyphen2, MutationTaster, and M-CAP software predicted that the p.Leu237Pro variant could affect gene products. No p.Arg819Ter variant was reported by searching the PubMed, ClinVar, and HGMD databases, indicating that we had identified a novel variant of *UNC-45A*. According to the ACMG guidelines, p.Arg819Ter was rated as possibly pathogenic (rating evidence: PVS1+PM2) and p.Leu237Pro was rated as uncertain (rating evidence: PM2+PM3+PP3). Sanger sequencing confirmed the presence of these two variants (Fig. 1b).

3.3. Prediction of Leu237Pro crystal structure

The UNC-45A protein belongs to the myosin coenzyme UNC45/CRO1/She4p (UCS) protein family and is composed of a C-terminal UCS domain, a non-highly conserved central domain, neck domain, and N-terminal tetratripeptide repeat (TPR) (Gazda et al., 2013). Homology analysis showed that the Leu237 residue of the UNC-45A protein is highly conserved among different species. Leu237Pro may cause a swing in the main chain of Ile236-Gly238 and destroy the hydrogen bond interactions between the amide nitrogen atom of the Leu237 main chain and the carbonyl oxygen atom of the Thr233 main chain. Simultaneously, Leu237Pro may also destroy the hydrophobic interaction between Leu237 and the side chain of nearby amino acid residues, causing a swing in the side chain of Gln201, thereby reducing the local structural stability (Fig. 2).

3.4. Mutation leads to the restricted expression of UNC-45A protein

The results of the WB experiment showed that the expression levels of UNC45A-WT and UNC45A-Leu237Pro group were higher than those in the NC-plasmid group. The protein expression of the UNC45A-Leu237Pro and UNC45A-Arg819Ter groups were significantly different from that of the UNC45A-WT group ($p < 0.001$). Compared with UNC45A-WT, the protein expression of the UNC45A-Leu237Pro group decreased by 27.4% and no expression of UNC45A-Arg819Ter histone was found (Fig. 3a).

Laser confocal microscopy showed that GFP was expressed in the cytoplasm of the samples from the UNC45A-WT group, while the expression of GFP was reduced in UNC45A-Leu237Pro, indicating that the expression of the mutant protein was reduced. No GFP expression was found in UNC45A-Arg819Ter (Fig. 3b). This is similar to the finding of the WB analysis, indicating that the two variants may lead to protein instability.

3.5. Laser confocal microscopy results

After fusing the C-terminus of the UNC-45A protein with a GFP label, the localization of UNC45A-WT and UNC45A-MUT in the cytoplasm was not affected by laser confocal microscopy. However, the expression of GFP in the UNC45A-Leu237Pro group decreased, and there was no expression of GFP in the UNC45A-Arg819Ter group, indicating that the variant may not affect the transport of the UNC-45A protein in cells (Fig. 3b).

4. Discussion

In the present study, we reported a neonate with OOHE. The baby had yellow skin since birth, and severe diarrhea symptoms were

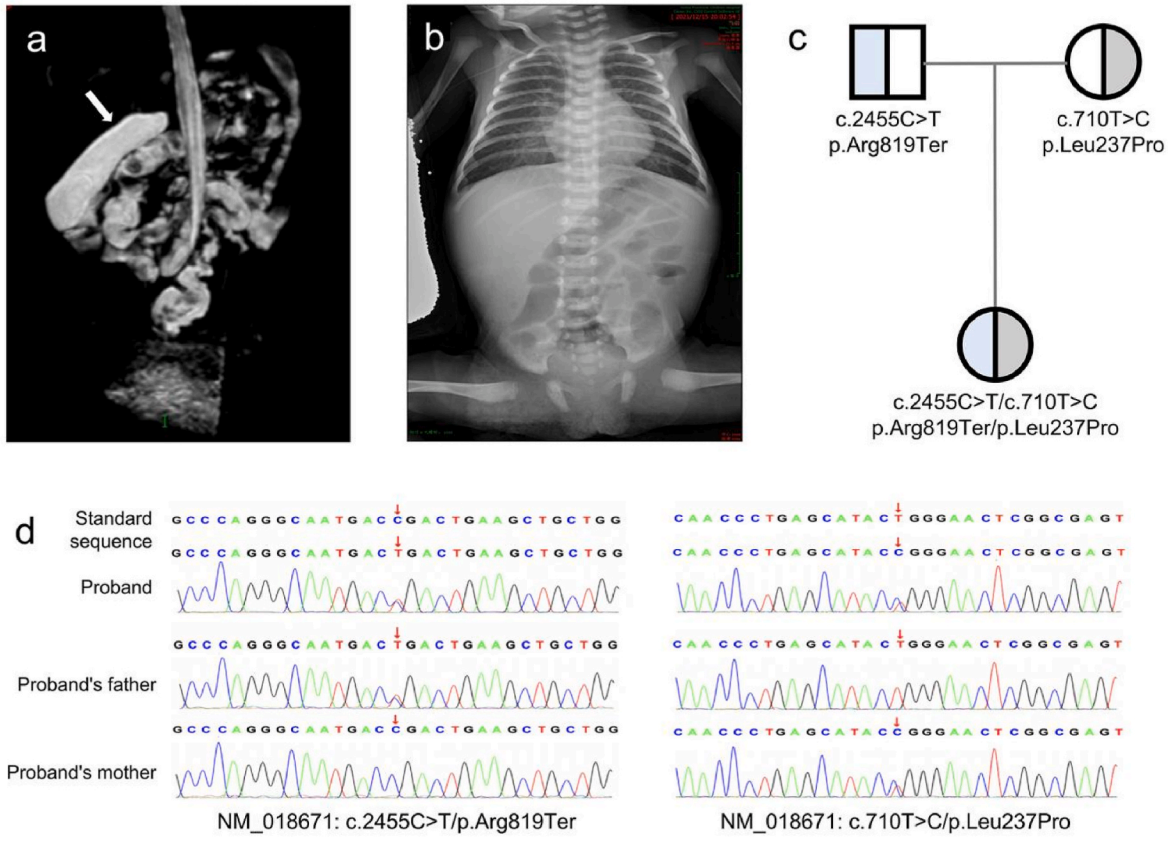

Fig. 1. The clinical information and gene detection results of the patient in this study. **a.** The magnetic resonance cholangiopancreatography of the baby showed that the gallbladder volume increased by approximately 56.00× 15.7 mm (shown by the white arrow), and the extrahepatic biliary system was poorly displayed. The intrahepatic bile duct showed a long T1T2 signal in tree shape, and the large vessels showed a flow void signal. **b.** The chest X-ray of the child showed that the markings of both lungs were fuzzy, with a strip-shaped fuzzy shadow. The peripherally inserted central catheter was inserted through the peripheral vein with the tube head at the T6 level. The abdominal shape was acceptable; the abdominal bowel was insufficiently inflated, a part of the bowel was slightly inflated and expanded, the intestinal space was thickened, and no calcification shadow was found in the abdomen. **c.** Gene detection results showed that the *UNC-45A* gene, in this patient, had compound heterozygous mutations, c.2455C>T and c.710T>C, of which the variation c.2455C>T was inherited from the father and the mutation c.710T>C was inherited from the mother. **d.** Sanger sequencing results confirmed the existence of these variants.

observed in the following days. According to biochemical indicators and imaging, the main symptoms were low birth weight, neonatal cholestasis, neonatal diarrhea, congenital heart disease (CHD), and electrolyte disorder. Through WES detection, we found that the patient's *UNC-45A* gene had compound heterozygous variants, Arg819Ter and Leu237Pro. The relevant public databases do not include these two variants according to the distribution frequency of the normal population. To date, only two papers reporting on patients with OOHE cases have been identified worldwide. Esteve et al. identified four OOHE patients from three families; these patients showed similar characteristics. Their symptoms mainly manifested as neonatal jaundice, cholestasis, diarrhea, as well as neurological hearing impairment in infancy. Other children may show mild mental and growth retardation. One of the two sisters showed symptoms of increased bone fragility. Loras et al. reported six OOHE patients. In addition to the common manifestations such as severe diarrhea, cholestasis, and abnormal bone fragility, this cohort developed other phenotypes such as cataracts, severe mental retardation, and abnormal behavior (Duclaux-Loras et al., 2022). Notably, our patient showed an atrial/ventricular septal defect, cardiac abnormalities of pulmonary hypertension, and brain structural abnormalities of bilateral ventricular widening. These clinical phenotypes of cardiac and brain structural abnormalities have not been reported in previous patients. *UNC-45A* is widely expressed in heart and brain tissues. Although we do not know the pathogenic mechanism whereby this gene leads to abnormal heart/brain structure, we suggest that OOHE patients should be alert to possible abnormalities in the heart/brain systems, in addition to typical abnormalities of the digestive or hepatobiliary system (Price et al., 2002).

The human *UNC-45A* gene is located in chromosome 15q26.1. The encoded UNC-45 myosin chaperone A belongs to the conserved UCS family of myosin (co-) chaperones and is homologous with UNC-45B in vertebrates (Li et al., 2022). As a myosin-specific chaperone, the UNC-45A protein can promote the folding of the myosin adenosine triphosphate domain and form a chaperone with heat shock protein 90 (Hsp90), resulting in human tumorigenesis (Eisa et al., 2019). However, the mechanism by which *UNC-45A* causes OOHE remains unclear. According to a recent study, the reduction or loss of UNC-45A protein function can lead to the reduction of myoglobin VB protein expression encoded by *MYO5B* and affect the development of microvilli and the localization function of the RAB11A protein during the recycling of endosomes. These abnormal physiological processes are associated with MVID pathogenesis (Li et al., 2022; Dhekne et al., 2014; Golachowska et al., 2012). Loras et al. showed typical MVID characteristics, such as dullness or absence of microvilli, accumulation of secretory granules, and formation of microvilli inclusion bodies in epithelial cells in the duodenal tissues of three patients with OOHE under an electron microscope (Duclaux-Loras et al., 2022). However, in previous zebrafish models with *unc-45a* and *myo5b* knockouts, the intestinal epithelium showed similar brush-like structure destruction (Anderson et al., 2008; Sidhaye et al., 2016). In addition, the restricted function of the myoglobin VB protein can lead to incorrect localization of intrahepatic bile acid transporters, leading to cholestasis symptoms (Gonzales et al.,

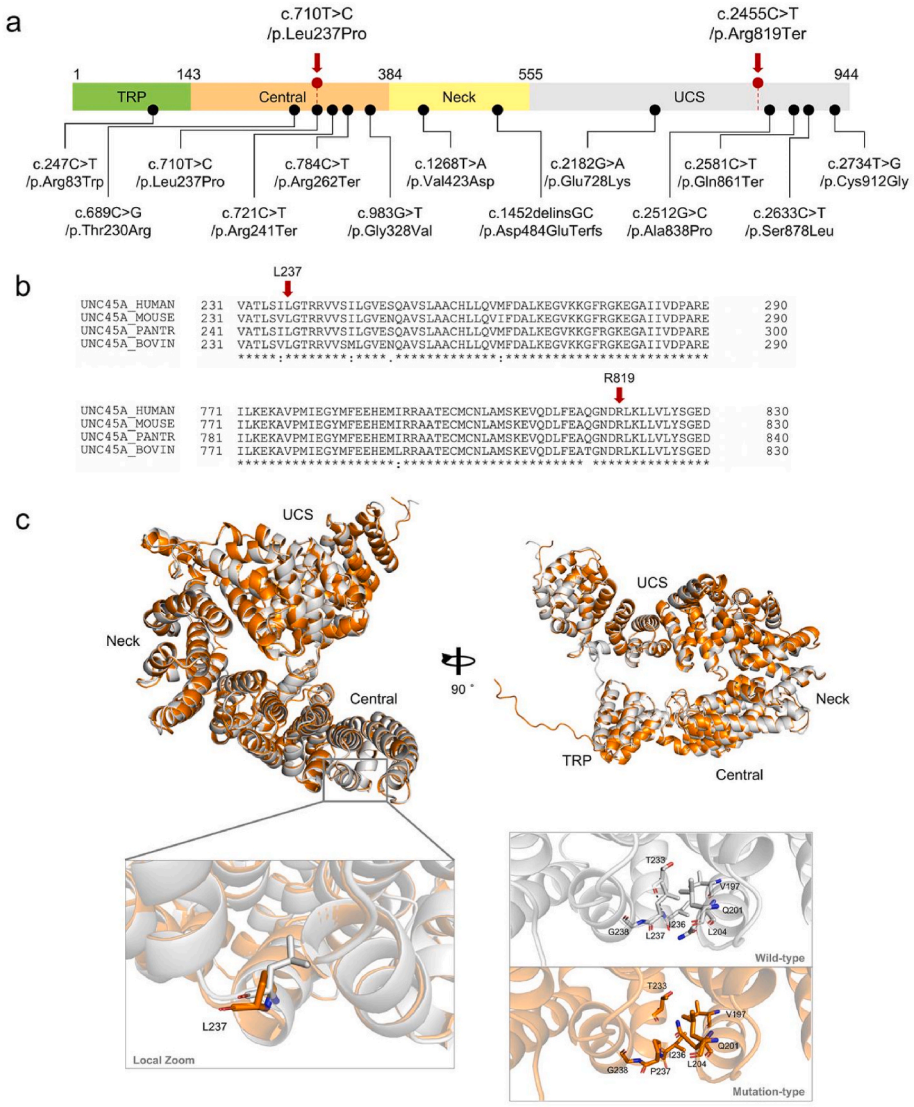

Fig. 2. Prediction and analysis results of the biological hazards of mutations in this study. **a.** Only two studies on OOHE patients have been reported worldwide, including 13 *UNC-45A* variants in 10 patients. Leu237Pro was reported in this study; this was located in the central domain. Arg819Ter is a novel variant of *UNC-45A* that is located in the C-terminal UCS domain; it was not reported in the present study. **b.** The two mutations we found were highly conserved among different species. **c.** The structure of UNC-45A consists of a C-terminal UCS domain, non-highly conserved central domain, neck domain, and N-terminal tetratripeptide repeat. Leu237Pro may destroy the hydrogen bond interaction with the carbonyl oxygen atom in the main chain of Thr233. Simultaneously, the mutation may also destroy the hydrophobic interaction between Leu237 and the side chain of nearby amino acid residues, resulting in the reduction of local structural stability.

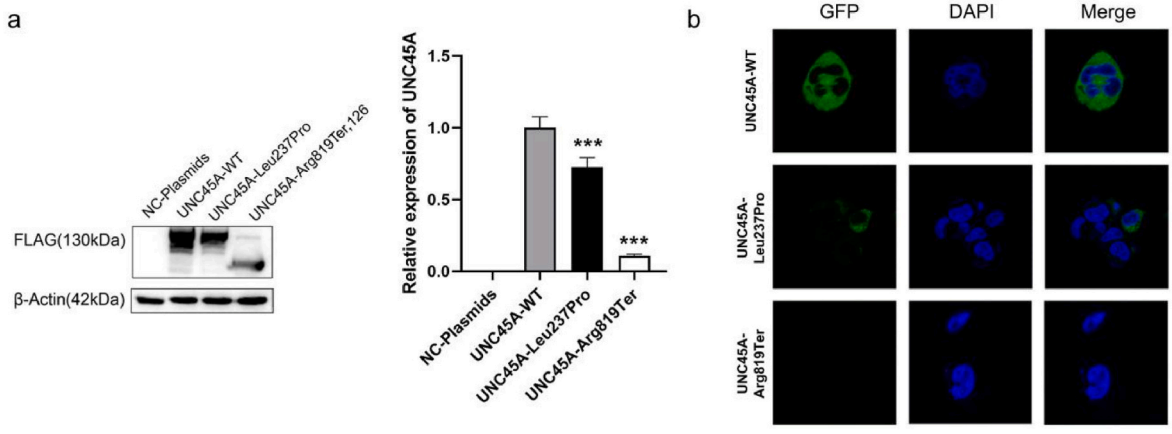

Fig. 3. Experimental results of the variation-related function. **a.** FLAG protein was fused with UNC-45A, and the expression of the UNC45A-Leu237Pro group was 27.4% lower than that of the UNC45A-WT group. No protein expression was found in the UNC45A-Arg819Ter group. **b.** The C-terminal fusion GFP label of the UNC-45A protein was used to observe that the localization of the UNC45A-WT and UNC45A-MUT groups in the cytoplasm were not affected by laser confocal microscopy. However, the expression of GFP in the UNC45A-Leu237Pro group was decreased, and there was no expression of GFP in the UNC45A-Arg819Ter group, indicating that the two variants may lead to protein instability.

2017; Overeem et al., 2020). These studies suggest that *UNC-45A* defects may cause MVID-like phenotypes, such as intractable diarrhea and cholestasis, by affecting the function of the myoglobin VB protein. However, the mechanisms underlying the development of bone fragility, neurogenic hearing loss, and other variable phenotypes in OOHE patients remain unclear.

To date, ten OOHE patients (from eight unrelated families) have been reported worldwide. Thirteen *UNC-45A* variants are related to OOHE, including one hotspot variant, Leu237Pro. The Leu237Pro homozygous variant of *UNC-45A* was found in three patients. Our patient also harbored this hotspot variant (Esteve et al., 2018; Duclaux-Loras et al., 2022). Leu237 is located in the central domain of the central armadillo repeat (ARM) sequence. The highly rigid central domain can be used as a molecular scaffold to adjust the orientation of the TPR and UCS domains flexibly, and the groove structure of the TPR domain plays an important role in identifying and binding chaperone proteins (Gazda et al., 2013; Scheufler et al., 2000). According to our constructed crystal structure analysis, the hydrogen bond between Leu237Pro and Thr233 was broken after the occurrence of Leu237Pro; further, the hydrophobic interaction with surrounding amino acid residues was destroyed, which may lead to a reduction in the rigidity of the central domain and affect biological functions. Notably, OOHE missense variants in both bi-alleles of *UNC-45A* mainly occur in the central domain. However, *UNC-45A* can be distributed in other domains because of the compound heterozygous variant, which is composed of loss-of-function and missense variants (Esteve et al., 2018; Duclaux-Loras et al., 2022). This suggests that the occurrence and phenotypic diversity of OOHE may be related to insufficient haploid doses or decreased protein function, but this requires further study.

OOHE has no specific treatment and is only symptomatic. Congenital diarrhea is usually the first symptom of OOHE. Because the abnormal gastrointestinal manifestations of OOHE and MVID are similar and may involve the same pathway, some treatment MVID treatments may be relevant to OOHE (Duclaux-Loras et al., 2022; Li et al., 2022). Total parenteral nutrition (TPN) supplements electrolytes and nutrients in OOHE patients but does not inhibit the occurrence of diarrhea (Duclaux-Loras et al., 2022). Concurrently, it has been proven that most infant deaths in patients with MVID are related to TPN complications. The most common causes of death in patients with MVID are catheter-related sepsis and hepatotoxic effects caused by long-term use of soybean lipids (Halac et al., 2011; Girard et al., 2014); therefore, OOHE patients should be cautious about the potential risk of infection caused by long-term TPN application. In addition, there have been many reports on the diarrhea symptoms of MVID patients after drug intervention, including the reduction in stool frequency and fecal volume after subcutaneous injection of octreotide and administration of racecadotril (Couper et al., 1989; Tran et al., 2017). However, owing to the small number of relevant patients who responded successfully to treatment, and the lack of long-term follow-up, the overall effective rate of drug intervention cannot be determined. Our patient was treated with an intravenous drip of nutrient solution (amino acids, 3 g/kg/d and fat emulsion, 2 g/kg/d) and maintenance of electrolyte stability (intravenous drip of sodium ions, 19 mmol/kg/d).

5. Conclusions

In conclusion, we conducted clinical research and genetic analysis of the first neonatal patient with OOHE in China. The patient presented with CDDs, cholestasis, CHD, brain structural abnormalities, and other symptoms shortly after birth. Gene detection showed that the *UNC-45A* gene of the patient had compound heterozygous variants. Our study expanded the phenotype and variant spectrum of OOHE. We compared the symptoms of diarrhea and cholestasis between OOHE and MVID and discussed the possibility that these conditions may share common pathological mechanisms. This suggests that OOHE should be considered as a possible explanation for severe diarrhea and cholestasis in newborns.

CRediT authorship contribution statement

Ying Kong: Writing – original draft, Designed the study, Wrote the manuscript. **Chaoqun Ye:** Writing – original draft, Designed the study, Wrote the manuscript. **Leyang Shi:** Designed the study. **Qingmei Dai:** Collecting data. **Ying Wang:** Collecting data. **Jun Hu:** Collecting data. **Xueyan Wu:** Collecting data. **Meiyu Shi:** Collecting data. **Xiaofeng Hu:** Revised the article. **Huizhi Huang:** Revised the article. All authors contributed to the article and approved the submitted version.

Declaration of competing interest

The authors declare that they have no conflicts of interest.

Data availability

Data will be made available on request.

Acknowledgements

We are very grateful to the family who participated in the study. This research was supported by the Young Scientific and Technological Talents Project of the Anhui Children's Hospital (ID: 20etyy002).

References

Anderson, M.J., Pham, V.N., Vogel, A.M., Weinstein, B.M., Roman, B.L., 2008. Loss of unc45a precipitates arteriovenous shunting in the aortic arches. Dev. Biol. 318, 258–267. https://doi.org/10.1016/j.ydbio.2008.03.022.

Baek, M., DiMaio, F., Anishchenko, I., Dauparas, J., Ovchinnikov, S., Lee, G.R., Wang, J., Cong, Q., Kinch, L.N., Schaeffer, R.D., Millán, C., Park, H., Adams, C., Glassman, C. R., DeGiovanni, A., Pereira, J.H., Rodrigues, A.V., van Dijk, A.A., Ebrecht, A.C., Opperman, D.J., et al., 2021. Accurate prediction of protein structures and interactions using a three-track neural network. Science 373, 871–876. https://doi.org/10.1126/science.abj8754.

Balistreri, W.F., Bezerra, J.A., Jansen, P., Karpen, S.J., Shneider, B.L., Suchy, F.J., 2005. Intrahepatic cholestasis: summary of an American association for the study of liver diseases single-topic conference. Hepatology 42, 222–235. https://doi.org/10.1002/hep.20729.

Barral, J.M., Hutagalung, A.H., Brinker, A., Hartl, F.U., Epstein, H.F., 2002. Role of the myosin assembly protein UNC-45 as a molecular chaperone for myosin. Science 295, 669–671. https://doi.org/10.1126/science.1066648.

Couper, R.T., Berzen, A., Berall, G., Sherman, P.M., 1989. Clinical response to the long acting somatostatin analogue SMS 201-995 in a child with congenital microvillus atrophy. Gut 30, 1020–1024. https://doi.org/10.1136/gut.30.7.1020.

Dhekne, H.S., Hsiao, N.H., Roelofs, P., Kumari, M., Slim, C.L., Rings, E.H., van Ijzendoorn, S.C., 2014. Myosin Vb and Rab11a regulate phosphorylation of ezrin in enterocytes. J. Cell Sci. 127, 1007–1017. https://doi.org/10.1242/jcs.137273.

Duclaux-Loras, R., Lebreton, C., Berthelet, J., Charbit-Henrion, F., Nicolle, O., Revenu de Courtils, C., Waich, S., Valovka, T., Khiat, A., Rabant, M., Racine, C., Guerrera, I.C., Baptista, J., Mahe, M.M., Hess, M.W., Durel, B., Lefort, N., Banal, C., Parisot, M., Talbotec, C., et al., 2022. UNC45A deficiency causes microvillus inclusion disease-like phenotype by impairing myosin VB-dependent apical trafficking. J. Clin. Invest. 132, e154997 https://doi.org/10.1172/JCI154997.

Eisa, N.H., Jilani, Y., Kainth, K., Redd, P., Lu, S., Bougrine, O., Abdul Sater, H., Patwardhan, C.A., Shull, A., Shi, H., Liu, K., Elsherbiny, N.M., Eissa, L.A., El-Shishtawy, M.M., Horuzsko, A., Bollag, R., Maihle, N., Roig, J., Korkaya, H., Cowell, J.K., et al., 2019. The co-chaperone UNC45A is essential for the expression of mitotic kinase NEK7 and tumorigenesis. J. Biol. Chem. 294, 5246–5260. https://doi.org/10.1074/jbc.RA118.006597.

Esposito, M.V., Comegna, M., Cernera, G., Gelzo, M., Paparo, L., Berni Canani, R., Castaldo, G., 2021. NGS gene panel analysis revealed novel mutations in patients with rare congenital diarrheal disorders. Diagnostics 11, 262. https://doi.org/10.3390/diagnostics11020262.

Esteve, C., Francescatto, L., Tan, P.L., Bourchany, A., De Leusse, C., Marinier, E., Blanchard, A., Bourgeois, P., Brochier-Armanet, C., Bruel, A.L., Delarue, A., Duffourd, Y., Ecochard-Dugelay, E., Hery, G., Huet, F., Gauchez, P., Gonzales, E., Guettier-Bouttier, C., Komuta, M., Lacoste, C., Fabre, A., 2018. Loss-of-Function mutations in UNC45A cause a syndrome associating cholestasis, diarrhea, impaired hearing, and bone fragility. Am. J. Hum. Genet. 102, 364–374. https://doi.org/10.1016/j.ajhg.2018.01.009.

Fawaz, R., Baumann, U., Ekong, U., Fischler, B., Hadzic, N., Mack, C.L., McLin, V.A., Molleston, J.P., Neimark, E., Ng, V.L., Karpen, S.J., 2017. Guideline for the evaluation of cholestatic jaundice in infants: joint recommendations of the north American society for pediatric gastroenterology, hepatology, and nutrition and the

European society for pediatric gastroenterology, hepatology, and nutrition. J. Pediatr. Gastroenterol. Nutr. 64, 154–168. https://doi.org/10.1097/MPG.0000000000001334.

Feldman, A.G., Sokol, R.J., 2013. Neonatal cholestasis. NeoReviews 14. https://doi.org/10.1542/neo.14-2-e63, 10.1542/neo.14-2-e63.

Gazda, L., Pokrzywa, W., Hellerschmied, D., Löwe, T., Forné, I., Mueller-Planitz, F., Hoppe, T., Clausen, T., 2013. The myosin chaperone UNC-45 is organized in tandem modules to support myofilament formation in C. elegans. Cell 152, 183–195. https://doi.org/10.1016/j.cell.2012.12.025.

Girard, M., Lacaille, F., Verkarre, V., Mategot, R., Feldmann, G., Grodet, A., Sauvat, F., Irtan, S., Davit-Spraul, A., Jacquemin, E., Ruemmele, F., Rainteau, D., Goulet, O., Colomb, V., Chardot, C., Henrion-Caude, A., Debray, D., 2014. MYO5B and bile salt export pump contribute to cholestatic liver disorder in microvillous inclusion disease. Hepatology 60, 301–310. https://doi.org/10.1002/hep.26974.

Golachowska, M.R., van Dael, C.M., Keuning, H., Karrenbeld, A., Hoekstra, D., Gijsbers, C.F., Benninga, M.A., Rings, E.H., van Ijzendoorn, S.C., 2012. MYO5B mutations in patients with microvillus inclusion disease presenting with transient renal Fanconi syndrome. J. Pediatr. Gastroenterol. Nutr. 54, 491–498. https://doi.org/10.1097/MPG.0b013e3182353773.

Goldberg, A., Mack, C.L., 2020. Inherited cholestatic diseases in the era of personalized medicine. Clin. Liver Dis. 15, 105–109. https://doi.org/10.1002/cld.872.

Gonzales, E., Taylor, S.A., Davit-Spraul, A., Thébaut, A., Thomassin, N., Guettier, C., Whitington, P.F., Jacquemin, E., 2017. MYO5B mutations cause cholestasis with normal serum gamma-glutamyl transferase activity in children without microvillous inclusion disease. Hepatology 65, 164–173. https://doi.org/10.1002/hep.28779.

Halac, U., Lacaille, F., Joly, F., Hugot, J.P., Talbotec, C., Colomb, V., Ruemmele, F.M., Goulet, O., 2011. Microvillous inclusion disease: how to improve the prognosis of a severe congenital enterocyte disorder. J. Pediatr. Gastroenterol. Nutr. 52, 460–465. https://doi.org/10.1097/MPG.0b013e3181fb4559.

Li, Q., Zhou, Z., Sun, Y., Sun, C., Klappe, K., van Ijzendoorn, S., 2022. A functional relationship between UNC45A and MYO5B connects two rare diseases with shared enteropathy. Cell. Mol. Gastroenterol. Hepatol. 14, 295–310. https://doi.org/10.1016/j.jcmgh.2022.04.006.

Overeem, A.W., Li, Q., Qiu, Y.L., Cartón-García, F., Leng, C., Klappe, K., Dronkers, J., Hsiao, N.H., Wang, J.S., Arango, D., van Ijzendoorn, S., 2020. A molecular mechanism underlying genotype-specific intrahepatic cholestasis resulting from MYO5B mutations. Hepatology 72, 213–229. https://doi.org/10.1002/hep.31002.

Price, M.G., Landsverk, M.L., Barral, J.M., Epstein, H.F., 2002. Two mammalian UNC-45 isoforms are related to distinct cytoskeletal and muscle-specific functions. J. Cell Sci. 115, 4013–4023. https://doi.org/10.1242/jcs.00108.

Richards, S., Aziz, N., Bale, S., Bick, D., Das, S., Gastier-Foster, J., Grody, W.W., Hegde, M., Lyon, E., Spector, E., Voelkerding, K., Rehm, H.L., ACMG Laboratory Quality Assurance Committee., 2015. Standards and guidelines for the interpretation of sequence variants: a joint consensus recommendation of the American College of medical genetics and genomics and the association for molecular pathology. Genet. Med. 17, 405–424. https://doi.org/10.1038/gim.2015.30.

Scheufler, C., Brinker, A., Bourenkov, G., Pegoraro, S., Moroder, L., Bartunik, H., Hartl, F. U., Moarefi, I., 2000. Structure of TPR domain-peptide complexes: critical elements in the assembly of the Hsp70-Hsp90 multichaperone machine. Cell 101, 199–210. https://doi.org/10.1016/S0092-8674(00)80830-2.

Sidhaye, J., Pinto, C.S., Dharap, S., Jacob, T., Bhargava, S., Sonawane, M., 2016. The zebrafish goosepimples/myosin Vb mutant exhibits cellular attributes of human microvillus inclusion disease. Mech. Dev. 142, 62–74. https://doi.org/10.1016/j.mod.2016.08.001.

Tran, L.C., Lazonby, G., Ellis, D., Goldthorpe, J., Iglesias, N., Steele, J., Zamvar, V., Puntis, J.W., Vora, R., 2017. Racecadotril may reduce diarrhoea in microvillous inclusion disease. J. Pediatr. Gastroenterol. Nutr. 64, e25–e26. https://doi.org/10.1097/MPG.0000000000001421.

Van den Broeck, J., Willie, D., Younger, N., 2009. The World Health Organization child growth standards: expected implications for clinical and epidemiological research. Eur. J. Pediatr. 168, 247–251. https://doi.org/10.1007/s00431-008-0796-9.